Spatial Correlation Model for Heterogeneous Cameras in Wireless Multimedia Sensor Networks

Moad Mowafi, Fahed Awad, Walid Aljoby
Faculty of Computer and Information Technology
Jordan University of Science and Technology
Irbid, Jordan
e-mail: {mowafi, fhawad}@just.edu.jo, waalgobi09@cit.just.edu.jo

***Abstract*—Collaborative in-network processing has shown to efficiently reduce the per-node processing and transmission requirements in wireless multimedia sensor networks. When the camera nodes are randomly distributed in an area of interest, it is very likely that their fields of view would overlap causing the corresponding visual information to be highly correlated. In applied wireless multimedia sensor networks, heterogeneous camera nodes with different sensing radii and angles of view are usually deployed, which has shown to enhance the overall network performance and lifetime. This paper introduces a new correlation model to exploit the correlation characteristics among heterogeneous camera nodes for wireless multimedia sensor networks. The proposed model, of which a closed-form analytical correlation function was derived, takes into consideration different sensing parameters of the camera nodes; such as the sensing radii and the angles of view. The simulation results demonstrated that the proposed model outperforms the state-of-the-art in terms of the accuracy of estimating the correlation characteristics, the information gain, and the distortion ratio.**

Keywords- spatial correlation; wireless multimedia sensor networks; joint entropy; heterogeneous cameras

I. INTRODUCTION

Wireless Multimedia Sensor Networks (WMSNs) are highly distributed and self-organized networks that are based on collaborative efforts of a large number of camera sensor nodes. WMSNs are increasingly used in many applications including environmental monitoring, surveillance, industrial automation, and health care monitoring [1][2]. The sensed data can be video, audio, still images, or scalar data. The camera sensor nodes are equipped with cameras that have the ability to capture visual data from the environment being monitored. The integrated camera has a directional sensing capability usually referred as the camera's Field of View (FoV), which defines the direction of viewing for a visible region emanating from the camera node.

Camera sensor nodes have limited storage, energy, processing, and transmission resources. Furthermore, visual information requires complicated processing techniques and high transmission bandwidth [1]. Therefore, the challenge is how to process and deliver a resource-intensive data as visual information with such limited resources.

In WMSN, the camera nodes can provide multiple views and resolutions of the area being observed [3]. Moreover, if the nodes are deployed randomly, a correlation among the visual information observed by cameras with overlapping fields of view is likely to occur [4]. Hence, the correlation characteristics can be exploited to design efficient collaborative in-network processing in order to decrease the volume of transferred multimedia data.

On the other hand, heterogeneity, in terms of camera sensing capability, has been considered as one of the characteristics of applied WMSNs, where the camera nodes have different sensing radii and angles of view. Cameras with different levels of resolution, coverage, and power consumption have been widely deployed in heterogeneous sensor networks in order to enhance the network performance and lifetime [5][6].

In this paper, we introduce a new spatial correlation model to determine the amount of correlation among heterogeneous camera nodes in WMSNs. The model considers different sensing parameters of the camera nodes including the sensing radius and the angle of view. In order to derive a closed-form analytical correlation function of the model, a novel technique was devised. This technique assumes that two virtual camera nodes exist at the far corners of the FoV to provide full coverage of the deployed camera's FoV.

This paper is organized as follows. In Section 2, the related research work is reviewed. In Section 3, the proposed spatial correlation model is introduced. In Section 4, the performance of the proposed model is evaluated and results are discussed. Section 5 concludes the paper.

II. RELATED WORK

The correlation of visual information detected by multiple camera nodes with overlapping FoVs was exploited in recent research works.

Image processing methods have been used to exploit the correlation of information observed by multiple camera nodes. For example, in [7], an image shape matching method was applied to find the overlap among spatially correlated images from neighboring sensor nodes, while in [8], correlated images are itemized using correspondence analysis. Nevertheless, image processing algorithms are complex and computationally intensive. Moreover, the performance of image processing techniques is application-dependent so that different kinds of images require different processing techniques [9]. Therefore, geometrical correlation

978-1-4673-5828-6/13/$31.00 ©2013 IEEE

methods have been used to exploit the correlation of visual information observed by multiple camera nodes.

In [10], a method for cooperative processing based on correlation was considered. It was assumed that the sensing areas compose of a set of discrete points and hence the correlation level of a pair of sensor nodes is estimated as the ratio of the overlapping discrete points to the total number of points in one sensor node's sensing area. However, this scheme works only with two camera nodes that are highly correlated.

In [11], it was assumed that the camera's FoV can be represented by trapezium in the ground plane. Two approaches were proposed to calculate the correlation coefficients of two cameras: grid-based and relative position-based, which were inspired by [12] and [13], respectively. The grid-based approach is very complex in that it requires a lot of time and energy. The relative position-based approach is lighter than the grid-based, but it does not consider the camera's sensing direction accurately as it produces close correlation characteristics for nodes with opposite directions.

In [4], a spatial correlation model (SCM) to determine the correlation characteristics between a set of camera nodes was proposed. Seven reference points in the 3D world coordinate system were selected and projected onto the camera's image plane. Hence, the correlation characteristics among given camera nodes could be estimated by comparing the projections of the reference points among the camera nodes. In this correlation model, it was assumed that all camera nodes have identical focal lengths. Therefore, this model is only valid for the case when the angles of view and sensing radii of the sensor nodes are the same.

Based on the above review, the state-of-the-art approaches to exploit the correlation characteristics of the overlapping FoV's are based on either processing-intense image processing techniques or spatial correlation techniques that are limited to homogeneous camera nodes.

Unlike the existing models, the model introduced in this paper takes into account the heterogeneity of the camera nodes in the sensing radius and the angle of view.

III. The Proposed Spatial Correlation Model

In this section, a heterogeneous spatial correlation model (HSCM) to exploit the correlation characteristics among heterogeneous camera sensor nodes is introduced. The system model is first presented and then a spatial correlation function is derived.

A. System Model

The camera node's FoV can be characterized by a directional sensing view that is similar to an isosceles triangle, as shown in Fig. 1, where the FoV is represented by four parameters: the camera position (P), the sensing radius (R_s), the angle of view (β), and the sensing direction (h) [10].

Our model is based on the system model defined by SCM [4]. It is assumed that the locations of the cameras, the focal lengths, and the sensing directions are known using some calibration and localization methods [14]–[16]. In SCM, it was assumed that the sensing process is characterized by 3D to 2D projection, where seven 3D points are selected as

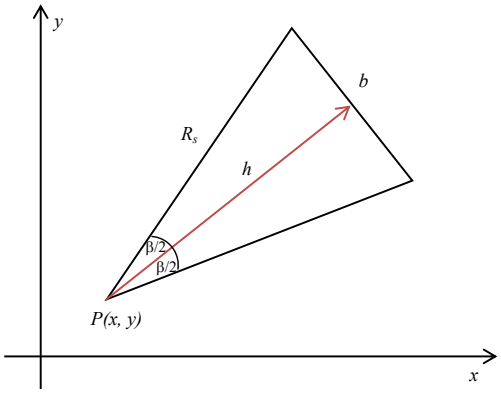

Figure 1. The camera node's FoV.

reference points to measure the 2D projected values on the deployed camera nodes. Fig. 2a shows the seven reference points, where the origin is at the center of the area of interest. Based on the coordinates of the reference points, the corresponding vectors can be used to compute the disparity among the images at different camera nodes. Fig. 2b shows three cameras deployed at three different locations in the world coordinate system. For Camera 1 and Camera 2, the principle axis passes through the center of the world coordinate system. For Camera 1, the sensing direction is along the x-axis, whereas for Camera 2, it rotates about the x-axis by an angle of θ. For Camera 3, the sensing direction rotates about the x-axis by an angle θ but the camera's principle axis does not pass through the center of the world coordinate system. For a set of camera nodes, the degree of correlation among them can be obtained by comparing the projections of the reference points on these camera nodes [4].

Unlike SCM, where it was assumed that all the camera nodes have the same focal length, our model takes into account different focal lengths for the cameras, and hence the sensing radii and angles of view are different. Accordingly, the reference points are projected at all corners of the camera's FoV; assuming two virtual cameras represent the base corners of the FoV triangle; as shown in Fig. 3. The projection of the reference points on the cameras changes, not only as the position and the sensing direction of the deployed camera change, but also as the sensing radius and angle of view change. By comparing the 2D projected values of the reference points at all corners of different cameras, the

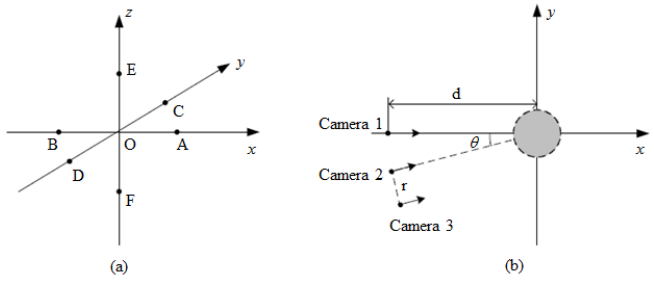

Figure 2. (a) The reference points in the area of interest and (b) The deployment of camera nodes [4].

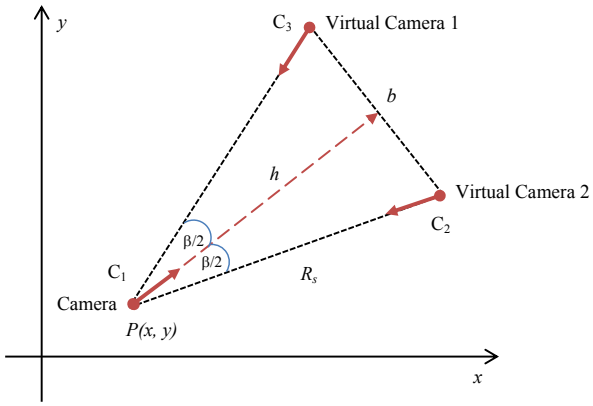

Figure 3. The camera node's FoV and the proposed virtual cameras.

correlation characteristics among them, can be accurately determined.

B. Geometrical Analysis

In the following, the projections of the reference points on the deployed camera as well as the virtual cameras are discussed.

To project the 3D reference points on a camera, a coordinate transformation of the world coordinate system (W) to the camera coordinate system is required. A coordinate transform is achieved by rotating the world coordinate (R_w) with angle θ around the x-axis, and then translating it (T_{wo}) in order to be mapped over the center of projection of the camera. Thus, using the coordinate transform, the relation between the coordinate vector of a scene point in the world coordinate system (P_w) and in the camera coordinate system (P_c) can be defined as:

$$P_c = R_w P_w + T_{w_o} \quad (1)$$

Three different settings of the geometry of the camera's FoV are studied with respect to the world x-axis. For each setting, we analyze the projection of the world reference points on the three corners of the FoV triangle as shown in Fig. 3.

1) Case 1: The optical center of the deployed camera is located at depth d from the origin of W, and its principle axis is along the x-axis or y-axis. Accordingly, the angle between the x-axis and the camera sensing direction (φ) can take one of the four values $\{0, \pi/2, \pi, 3\pi/2\}$.

To project the reference points on the deployed camera, we apply the coordinate transform equation as follows: Rotate W counterclockwise by θ, the angle between the W's negative x-axis and the sensing direction, and then translate the system by a length of d along the negative x-axis.

To project the reference points on the virtual cameras, we apply the coordinate transform equation taking into consideration the locations of the cameras with respect to the origin of W. Here, Virtual Camera 1 and Virtual Camera 2 represent Camera 3 in Fig. 2b, where the optical center for both cameras is at depth $d_v = (h - d)/\cos(\beta/2)$, and the distance from the origin to the principle axis of Virtual Camera 1 and Virtual Camera 2 is $r_{v1} = b/2 - d_v \sin(\beta/2)$ and $r_{v2} = b/2 + d_v \sin(\beta/2)$, respectively.

2) Case 2: The optical center of the deployed camera is located at depth d from the origin of W, and its principle axis passes through the origin of W; like Camera 2 in Fig. 2b. Accordingly, φ can take any value from the interval $(0, 2\pi)\backslash\{\pi/2, \pi, 3\pi/2\}$.

To project the reference points on the deployed camera, we apply the coordinate transform equation as follows: Rotate W counterclockwise by θ, and then translate the system by a length of d along the negative x-axis.

As in Case 1, Virtual Camera 1 and Virtual Camera 2 represent Camera 3 in Fig. 2b, where $d_v = h - d$ and $r_{v1} = r_{v2} = b/2$. Accordingly, we apply the coordinate transform equation to project the reference points on the virtual cameras.

3) Case 3: The optical center of the deployed camera is located at depth d from the origin of W, its principle axis does not pass though the origin of W, and the distance from the origin to its principle axis is r, as Camera 3 in Fig. 2b. Accordingly, φ can take any value from the interval $(0, 2\pi)\backslash\{\pi/2, \pi, 3\pi/2\}$.

To project the reference points on the deployed camera, we apply the coordinate transform equation as follows: Rotate W counterclockwise θ, and translate the system by a length of d along the negative x-axis, and then translate the resultant system by a length of r along the camera's positive y-axis.

As in the previous cases, Virtual Camera 1 and Virtual Camera 2 represent Camera 3 in Fig. 2b, where $d_v = h - d$, $r_{v1} = b/2 - r$, and $r_{v2} = b/2 + r$. Accordingly, we apply the coordinate transform equation to project the reference points on both cameras.

After obtaining the coordinates of the reference points in the camera 3D coordinate system, the projection of these reference points on a camera is obtained by mapping them onto the 2D image plane of the camera using the pinhole camera model [17].

C. The Spatial Correlation Function

In general, the following steps are required to determine the correlation between any two deployed camera nodes: Camera i with parameters $(d_i, \varphi_i, r_i, \beta_i)$ and Camera j with parameters $(d_j, \varphi_j, r_j, \beta_j)$, where d_i is the depth, at which Camera i is located from the origin of W, φ_i is the angle between the W's x-axis and the sensing direction of Camera i, r_i is the distance from the origin of W to the principle axis of Camera i, and β_i is the angle of view of Camera i.

1. Calculate the disparity (γ) between Camera i and Camera j at each corner of the FoV triangle (C_1, C_2, and C_3 in Fig. 3), as the average distance of the reference vectors:

$$\gamma_{C_1(ij)} = \frac{1}{4}\left(\left|\frac{-d_i \sin\theta_1^i - r_i\cos\theta_1^i}{d_i + \cos\theta_1^i} - \frac{-d_j \sin\theta_1^j - r_j\cos\theta_1^j}{d_j + \cos\theta_1^j}\right| + \left|\frac{d_i \sin\theta_1^i + r_i\cos\theta_1^i}{d_i - \cos\theta_1^i} - \frac{d_j \sin\theta_1^j + r_j\cos\theta_1^j}{d_j - \cos\theta_1^j}\right| + \left|\frac{d_i \cos\theta_1^i - r_i\sin\theta_1^i}{d_i + \sin\theta_1^i} - \frac{d_j \cos\theta_1^j - r_j\sin\theta_1^j}{d_j + \sin\theta_1^j}\right| + \left|\frac{-d_i \cos\theta_1^i + r_i\sin\theta_1^i}{d_i - \sin\theta_1^i} - \frac{-d_j \cos\theta_1^j + r_j\sin\theta_1^j}{d_j - \sin\theta_1^j}\right|\right) \quad (2)$$

$$\gamma_{C_2(ij)} = \frac{1}{4}\left(\left|\frac{-D_2^i(\alpha)\sin\theta_2^i + R_2^i(\tau)\cos\theta_2^i}{D_2^i(\alpha) + \cos\theta_2^i} - \frac{-D_2^j(\alpha)\sin\theta_2^j + R_2^j(\tau)\cos\theta_2^j}{D_2^j(\alpha) + \cos\theta_2^j}\right| + \left|\frac{D_2^i(\alpha)\sin\theta_2^i - R_2^i(\tau)\cos\theta_2^i}{D_2^i(\alpha) - \cos\theta_2^i} - \frac{D_2^j(\alpha)\sin\theta_2^j - R_2^j(\tau)\cos\theta_2^j}{D_2^j(\alpha) - \cos\theta_2^j}\right| + \left|\frac{D_2^i(\alpha)\cos\theta_2^i + R_2^i(\tau)\sin\theta_2^i}{D_2^i(\alpha) + \sin\theta_2^i} - \frac{D_2^j(\alpha)\cos\theta_2^j + R_2^j(\tau)\sin\theta_2^j}{D_2^j(\alpha) + \sin\theta_2^j}\right| + \left|\frac{-D_2^i(\alpha)\cos\theta_2^i - R(\tau)\sin\theta_2^i}{D_2^i(\alpha) - \sin\theta_2^i} - \frac{-D_2^j(\alpha)\cos\theta_2^j - R_2^j(\tau)\sin\theta_2^j}{D_2^j(\alpha) - \sin\theta_2^j}\right|\right) \quad (3)$$

$$\gamma_{C_3(ij)} = \frac{1}{4}\left(\left|\frac{-D_3^i(\alpha)\sin\theta_3^i - R_3^i(\tau)\cos\theta_3^i}{D_3^i(\alpha) + \cos\theta_3^i} - \frac{-D_3^j(\alpha)\sin\theta_3^j - R_3^j(\tau)\cos\theta_3^j}{D_3^j(\alpha) + \cos\theta_3^j}\right| + \left|\frac{D_3^i(\alpha)\sin\theta_3^i + R_3^i(\tau)\cos\theta_3^i}{D_3^i(\alpha) - \cos\theta_3^i} - \frac{D_3^j(\alpha)\sin\theta_3^j + R_3^j(\tau)\cos\theta_3^j}{D_3^j(\alpha) - \cos\theta_3^j}\right| + \left|\frac{D_3^i(\alpha)\cos\theta_3^i - R_3^i(\tau)\sin\theta_3^i}{D_3^i(\alpha) + \sin\theta_3^i} - \frac{D_3^j(\alpha)\cos\theta_3^j - R_3^j(\tau)\sin\theta_3^j}{D_3^j(\alpha) + \sin\theta_3^j}\right| + \left|\frac{-D_3^i(\alpha)\cos\theta_3^i + R_3^i(\tau)\sin\theta_3^i}{D_3^i(\alpha) - \sin\theta_3^i} - \frac{-D_3^j(\alpha)\cos\theta_3^j + R_3^j(\tau)\sin\theta_3^j}{D_3^j(\alpha) - \sin\theta_3^j}\right|\right) \quad (4)$$

where,

$$\theta_1^i = \begin{cases} \pi + \varphi_i, & \varphi_i \in \{0, \pi/2\} \\ \varphi_i - \pi, & \varphi_i \in \{\pi, 3\pi/2\} \end{cases}, \quad \text{for Case 1}$$

$$\theta_1^i = \begin{cases} \pi + \varphi_i, & \varphi_i \in (0, \pi)\backslash\{\pi/2\} \\ \varphi_i - \pi, & \varphi_i \in (\pi, 2\pi)\backslash\{3\pi/2\} \end{cases}, \quad \text{for Cases 2 and 3}$$

$$\theta_2^i = \theta_3^i = \varphi_i + \beta_i/2\,, \quad \varphi_i \in \{0, \pi/2, \pi, 3\pi/2\}, \quad \text{for Case 1}$$

$$\theta_2^i = \theta_3^i = \varphi_i,\ \varphi_i \in (0, 2\pi)\backslash\{\pi/2, \pi, 3\pi/2\}, \text{ for Cases 2 and 3}$$

$$D_2^i(\alpha) = D_3^i(\alpha) = \left(\frac{h_i - d_i}{\cos(\alpha)}\right), \quad \alpha = \begin{cases} \beta_i/2 & \text{Case 1} \\ 0 & \text{Cases 2 and 3} \end{cases}$$

$$R_2^i(\tau) = b_i/2 + \tau, \quad \tau = \begin{cases} D_2^i(\beta_i/2)\sin(\beta_i/2)\,, & \text{Case 1} \\ 0, & \text{Case 2} \\ r_i, & \text{Case 3} \end{cases}$$

$$R_3^i(\tau) = b_i/2 - \tau, \quad \tau = \begin{cases} D_3^i(\beta_i/2)\sin(\beta_i/2)\,, & \text{Case 1} \\ 0, & \text{Case 2} \\ r_i, & \text{Case 3} \end{cases}$$

2. Compute the average disparity among the three corners in order to find the disparity between the two camera nodes:

$$\gamma = \frac{1}{3}\left(\gamma_{C_1(ij)} + \gamma_{C_2(ij)} + \gamma_{C_3(ij)}\right) \quad (5)$$

3. Calculate the correlation coefficient (ρ) as the complement of γ:

$$\rho = 1 - \gamma \quad (6)$$

IV. Performance Evaluation

In this section, the performance of HSCM is evaluated and compared against SCM in terms of the accuracy of estimating the correlation coefficients, and the two performance metrics: the joint entropy and the distortion ratio.

A. Correlation Coefficients Estimation

To evaluate how accurate HSCM can estimate the correlation coefficients, two simulation experiments were conducted. In each experiment, 24 camera nodes were uniformly deployed around the center of an area of interest such that the difference in the sensing direction between any two neighboring nodes is θ=15˚ and the depth for all nodes from the center is 10m. In the first experiment, it was assumed that the camera nodes are homogeneous, having the same focal length, and hence the same angle of view. In the second experiment, it was assumed that the cameras are heterogeneous with different angles of view.

1) Homogeneous Camera Nodes: In this experiment, both models were applied to the 24 camera nodes, for each of which a 24×24 correlation coefficient matrix was generated, where each row represents the correlation coefficients of one camera node. For example, the first row represents the coefficients of the camera node with sensing direction along the x-axis (i.e.; θ=0˚), whereas the second row represents the coefficients of the camera node with the sensing direction rotating about the x-axis by angle of θ=15˚. To illustrate the relationship clearly, the correlation coefficients for the camera node with θ=15˚ were drawn with respect to all other camera nodes; as shown in Fig. 4.

Fig. 4 shows the extracted correlation coefficients for

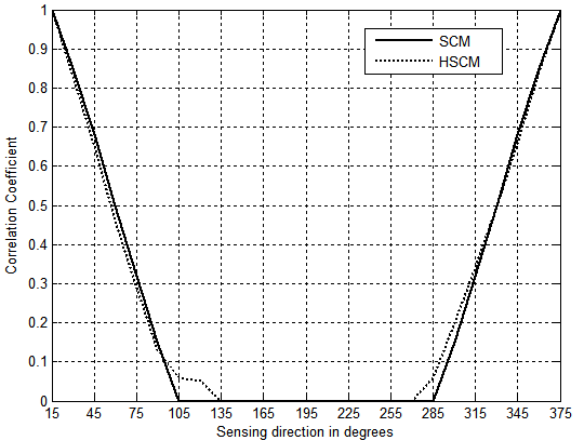

Figure 4. The correlation coefficients between the camera node with θ=15˚ and each of the 24 homogeneous camera nodes.

both SCM and HSCM. As shown, the correlation coefficient curves pass through three discrete parts from left to right. In the first part, it is noted that the correlation coefficient decreases whenever the sensing direction increases, in the second part, the correlation coefficient stays at zero, and in the third part, it increases as the sensing direction increases. It can be concluded that the correlation coefficient increases whenever the difference in the sensing direction among the nodes decreases and goes to zero as long as the nodes have perpendicular or opposite sensing directions. As shown, both models generate similar results because they are applied to homogenous camera nodes.

2) Heterogeneous Camera Nodes: In this experiment, we applied both models to the 24 heterogeneous camera nodes with different angles of view. As the camera's angle of view gets wider, more world points are projected onto the camera image plane and vice versa. To see how this affects the correlation characteristics among the camera nodes, we assume that the camera with sensing direction θ=15˚ has a fixed angle of view (AoV=40˚), while the other camera nodes with sensing directions θ=30˚, 45˚, 60˚, and 75˚ change their angles of view between AoV=50˚ to AoV=80˚. For each AoV, the correlation coefficients between the camera node with θ=15˚ and the rest of the camera nodes were extracted.

Fig. 5 compares the extracted correlation coefficients of SCM and HSCM. For SCM, the correlation coefficients for each sensing direction are the same for all values of AoV because it compares the difference among the nodes only in terms of position without considering the variations in the AoV. Therefore, SCM provides inaccurate correlation characteristics among the nodes with different AoVs. On the other hand, the correlation coefficients produced by HSCM change whenever the AoVs change. Specifically, the correlation between the node with θ=15˚ and any of the other nodes increases whenever the two nodes have close AoVs. For instance, the node with θ=30˚ and the node with θ=15˚ are more correlated when AoV=50˚ than when AoV=60˚, 70˚, or 80˚. Also, the two nodes are more correlated when AoV=60˚ than when AoV=70˚ or 80˚, and so forth. This is because the overlapped world points between the node with AoV=40˚ and the node with AoV=50˚ are more than those for the nodes with AoV=60˚, 70˚, or 80˚, with respect to the total number of world points in one camera's FoV. Similarly, the ratio of the overlapped world points when AoV=60˚ is more than that when AoV=70˚ or 80˚.

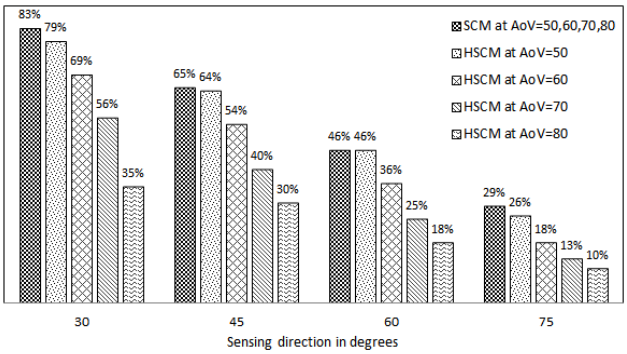

Figure 5. The correlation coefficients between the camera node with θ=15˚ and 4 heterogeneous camera nodes with different AoV's.

B. Joint Entropy

We used the joint entropy as a performance metric to measure how much information can be gained from multiple correlated camera nodes. The joint entropy is inversely proportional to the correlation coefficient between two camera nodes. That is, the less correlated the two camera nodes are, the larger the amount of information gained.

In the simulation environment, 100 heterogeneous camera nodes were deployed in a 200m×200m sensor field, for which the observed area of interest was assumed to be located at the center of the field. The nodes had different AoVs (∅=20˚–100˚) and different depths (d=10–50m) from the center of the area of interest. It was also assumed that a sink node selects a specific number of camera nodes (M=2–100) out of all nodes in the network to report their observed information. The joint entropy (i.e.; the information gain) is calculated using the joint entropy estimation algorithm discussed in [4]. The camera nodes are selected using two schemes: random-based and correlation-based. In the random selection scheme, M camera nodes were randomly selected. This experiment was repeated 100 times for each M and the average joint entropy was calculated. In the correlation-based selection scheme, the least correlated M nodes were selected using the correlation-based camera selection algorithm used in [4] so that the information gain is maximized. For comparison purposes, the correlation-based selection scheme was implemented using both SCM and HSCM.

Fig. 6 compares the estimated joint entropy for both SCM and HSCM, in addition to the random selection scheme (RSS). As shown, the joint entropy increases as the number of selected camera nodes increases, and accordingly the gain of the reported information increases. HSCM clearly outperforms SCM and RSS as it always achieves higher joint entropy for each value of M, with the exception when all the camera nodes are selected (i.e.; when M=100). According to the numerical results, the average increase in the joint

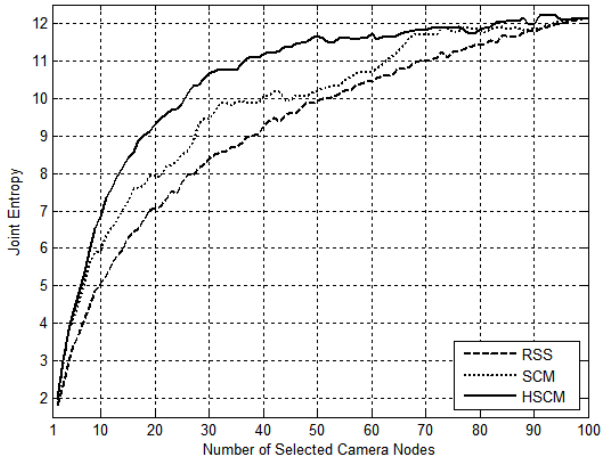

Figure 6. A Comparsion of estimated joint entropy.

entropy for SCM and HSCM with respect to RSS is 3.7% and 14.4%, respectively.

C. Distortion Ratio

The distortion ratio was used as a performance metric to measure the percentage of information loss due to selecting only a subset of the camera nodes to report their information to the sink; compared to the maximum amount of information obtained if all nodes are selected. The same simulation environment and camera selection schemes described in the previous section were used in this section.

Fig. 7 compares the distortion ratio of SCM and HSCM, in addition to RSS. It is shown that as the number of selected camera nodes increases, the distortion ratio decreases and accordingly the information loss decreases. HSCM clearly outperforms SCM and RSS as it always has lower distortion ratio for each value of M, with the exception when all the camera nodes are selected (i.e.; when M=100). For instance, if an application needs 40 camera nodes to report their information to the sink, then HSCM causes only 8.4% information loss, whereas SCM and RSS cause 18.5% and 23.4% information loss, respectively. Thus, the average percent improvement on the distortion ratio of HSCM with respect to SCM is 54.6%.

V. Conclusion

This paper presents a new efficient geometrical correlation model to estimate the correlation characteristics among multiple heterogeneous camera nodes for wireless multimedia sensor networks. The performance of the proposed model was evaluated and compared against the state-of-the-art models in terms of the accuracy of estimating the correlation characteristics, the joint entropy, and the distortion ratio. In terms of estimating the correlation coefficients, the proposed model enhances the estimation of the correlation characteristics, especially when the deployed camera nodes are heterogeneous with different parameters. In terms of the joint entropy and the distortion ratio, the proposed model can select the lowest number of camera sensor nodes to report specific bound of information to the sink and yield the highest level of information gain with the lowest distortion ratio for the received information by the sink. The correlation characteristics obtained from our model can be potentially used to develop efficient collaborative multimedia in-network processing and cross-layering algorithms.

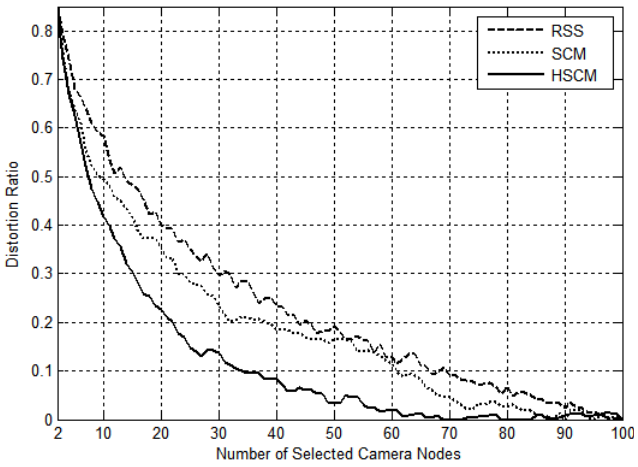

Figure 7. A comparsion of estimated distortion ratio.

References

[1] I. F. Akyildiz, T. Melodia, and K. R. Chowdhury, "A survey on wireless multimedia sensor networks," Comput. Networks, vol. 51, no. 4, pp. 921-960, 2007.

[2] S. Misra, M. Reisslein, and G. Xue, "A survey of multimedia streaming in wireless sensor networks," Commun. Surveys & Tutorials, IEEE, vol. 10, no. 4, pp. 18-39, 2008.

[3] R. Cucchiara, "Multimedia surveillance systems," Proc. 3rd ACM Int. Workshop Video Surveillance & Sensor Networks (VSSN '05), ACM, 2005, pp. 3-10.

[4] R. Dai and I. F. Akyildiz, "A spatial correlation model for visual information in wireless multimedia sensor networks," IEEE Trans. Multimedia, vol. 11, no. 6, pp. 1148-1159, 2009.

[5] Y. Wu and X. Wang; "Achieving full view coverage with randomly-deployed heterogeneous camera sensors," Proc. 32nd IEEE Int. Conf. Distributed Computing Systems (ICDCS 2012), IEEE, June 2012, pp.556-565.

[6] M. Meingast et al., "Fusion-based localization for a heterogeneous camera network," Proc. 2nd ACM/IEEE Int. Conf. Distributed Smart Cameras (ICDSC 2008), IEEE, Sept. 2008, pp.1-8.

[7] M. Wu and C. W. Chen, "Collaborative image coding and transmission over wireless sensor networks," EURASIP J. Advances in Signal Process., vol. 2007, no. 70481, 2007.

[8] R. Wagner, R. Nowak, and R. Baraniuk, "Distributed image compression for sensor networks using correspondence analysis and super-resolution,", 2003.. Proc. Int. Conf. Image Processing (ICIP 2003), IEEE, Sept. 2003, pp. 597-600.

[9] R. C. Gonzalez, R. E. Woods, and S. L. Eddins, Digital Image Processing Using MATLAB, New Jersey: Prentice Hall, 2004.

[10] H. Ma and Y. Liu, "Correlation based video processing in video sensor networks," IEEE Int. Conf. Wireless Networks, Communications and Mobile Computing, IEEE, June 2005, pp. 987-992.

[11] C. Han, L. Sun, F. Xiao, J. Guo, and R. Wang, "FoVs correlation model for wireless multimedia sensor networks based on three dimensional perception," Advances in Inform. Sci. and Service Sciences, vol. 4, no. 3, pp. 27-34, 2012.

[12] P. Wang, R. Dai, and I. F. Akyildiz, "A spatial correlation-based image compression framework for wireless multimedia sensor networks," IEEE Trans. Multimedia, vol. 13, no. 2, pp. 388-401, 2011.

[13] M. Alaei and J. M. Barcelo-Ordinas, "A method for clustering and cooperation in wireless multimedia sensor networks," Sensors, vol. 10, no. 4, pp. 3145-3169, 2010.

[14] A. Barton-Sweeney, D. Lymberopoulos, and A. Sawides, "Sensor localization and camera calibration in distributed camera sensor networks," 3rd Int. Conf. Broadband Communications, Networks and Systems (BROADNETS 2006), IEEE, Oct. 2006, pp.1-10.

[15] S. Funiak, C. Guestrin, M. Paskin, and R. Sukthankar, "Distributed localization of networked cameras," Proc. 5th Int. Conf. Information Processing in Sensor Networks (IPSN 2006), IEEE, July 2006, pp.34-42.

[16] D. Devarajan, Z. Cheng, and R. J. Radke, "Calibrating distributed camera networks," Proc. IEEE, vol. 96, no. 10, pp. 1625-1639, Oct. 2008.

[17] D. A. Forsyth and J. Ponce, Computer Vision: A Modern Approach, New Jersey: Prentice Hall, 2002.